Atmos. Chem. Phys., 15, 3241–3255, 2015
www.atmos-chem-phys.net/15/3241/2015/
doi:10.5194/acp-15-3241-2015


Atmospheric Chemistry and Physics
Open Access

# Spaceborne observations of the lidar ratio of marine aerosols

**K. W. Dawson[1], N. Meskhidze[1], D. Josset[2,*], and S. Gassó[3]**

[1]Marine, Earth, and Atmospheric Science, North Carolina State University, Raleigh, NC, USA
[2]Science Systems and Applications, Inc./NASA Langley Research Center, Hampton, VA, USA
[3]GESTAR/Morgan State University, Goddard Space Flight Center, Greenbelt, MD, USA
[*]now at: Naval Research Laboratory, Stennis Space Center, Mississippi, USA

*Correspondence to:* N. Meskhidze (nmeskhidze@ncsu.edu)

Received: 29 October 2013 – Published in Atmos. Chem. Phys. Discuss.: 6 January 2014
Revised: 23 February 2015 – Accepted: 26 February 2015 – Published: 23 March 2015

**Abstract.** Retrievals of aerosol optical depth (AOD) from the Cloud-Aerosol Lidar with Orthogonal Polarization (CALIOP) satellite sensor require the assumption of the extinction-to-backscatter ratio, also known as the lidar ratio. This paper evaluates a new method to calculate the lidar ratio of marine aerosols using two independent sources: the AOD from the Synergized Optical Depth of Aerosols (SODA) project and the integrated attenuated backscatter from CALIOP. With this method, the particulate lidar ratio can be derived for individual CALIOP retrievals in single aerosol layer, cloud-free columns over the ocean. Global analyses are carried out using CALIOP level 2, 5 km marine aerosol layer products and the collocated SODA nighttime data from December 2007 to November 2010. The global mean lidar ratio for marine aerosols was found to be 26 sr, roughly 30 % higher than the current value prescribed by the CALIOP standard retrieval algorithm. Data analysis also showed considerable spatiotemporal variability in the calculated lidar ratio over the remote oceans. The calculated marine aerosol lidar ratio is found to vary with the mean ocean surface wind speed ($U_{10}$). An increase in $U_{10}$ reduces the mean lidar ratio for marine regions from $32 \pm 17$ sr (for $0 < U_{10} < 4\,\mathrm{m\,s^{-1}}$) to $22 \pm 7$ sr (for $U_{10} > 15\,\mathrm{m\,s^{-1}}$). Such changes in the lidar ratio are expected to have a corresponding effect on the marine AOD from CALIOP. The outcomes of this study are relevant for future improvements of the SODA and CALIOP operational product and could lead to more accurate retrievals of marine AOD.

## 1 Introduction

Marine aerosols are produced through primary emission of sea spray particles and oxidation of phytoplankton-produced dimethylsulfide and biogenic volatile organic carbon. Radiative forcing by marine aerosol comprises a significant portion of the global energy budget. Studies have shown that marine aerosol optical depth (AOD) is approximately 0.15 and, likewise, the contribution of marine aerosol to cloud condensation nuclei is about 60 $\mathrm{cm^{-3}}$ (Kaufman et al., 2002; Lewis and Schwartz, 2004). Thus, marine aerosol is an important natural contributor to global aerosol burden affecting both direct (i.e., extinction of solar radiation via scattering and absorption) and indirect (i.e., cloud lifetime and frequency) radiative forcing of climate. As marine aerosols contribute considerably to the preindustrial, natural background and provide the base line on top of which anthropogenic forcing should be quantified, it is very important to properly characterize marine aerosol burden and its spatiotemporal distribution. The incomplete characterization of background aerosols, of which marine particles are a part, was shown to contribute large uncertainty in anthropogenic aerosol forcing calculations and climate simulations (Ghan et al., 2001; Hoose et al., 2009; Wang and Penner, 2009; Meskhidze et al., 2011; Westervelt et al., 2012; Carslaw et al., 2013).

Aerosols over the remote oceans come from natural continental (e.g., mineral dust and biomass burning) and human-induced pollution (Andreae, 2007) in addition to marine sources. Therefore, knowing horizontal and vertical distribution as well as speciation of aerosols becomes extremely important for the correct quantification of marine aerosol radiative properties. The last decade has produced a large body

of information regarding the sources and composition of marine aerosol, resulting in a reassessment of the complex role that marine aerosols play in climate and various geophysical phenomena. Passive satellite instruments like the Seaviewing Wide Field-of-view Sensor (SeaWiFS), the MODerate resolution Imaging Spectroradiometer (MODIS), the Multi-angle Imaging SpectroRadiometer, and the ground-based AErosol RObotic NETwork (AERONET) have contributed immensely to quantitative characteristics of marine aerosol in terms of AOD (the column integrated aerosol extinction), size distribution information, and spectral optical properties. Although passive instruments have been useful for developing a basic picture of marine aerosol distribution, they supply limited information on aerosol speciation and very little data related to aerosol distribution in the vertical column. The introduction of the Cloud-Aerosol Lidar with Orthogonal Polarization (CALIOP) onboard the Cloud-Aerosol Lidar and Infrared Pathfinder Satellite Observations (CALIPSO) platform has eliminated some of the assumptions made by the passive instruments and has provided a more complete picture of the global aerosol distribution wanted by climate scientists. However, CALIOP is an elastic backscatter lidar with no molecular filtering capability and therefore requires the assumption of an extinction-to-backscatter ratio, also known as the lidar ratio, to infer extinction from attenuated backscatter measurements. Depending on the microphysical properties of the aerosol, the lidar ratio can have a wide range of values and therefore a straightforward a priori solution within some reasonable uncertainty range is generally unobtainable without various assumptions or constraints. Theoretical calculations for the lidar ratio can be performed when the physicochemical properties and the size distribution of the particles at the different heights in the vertical column are known; however, the fulfillment of these requirements would make the lidar measurements unnecessary (Ackermann, 1998). The typical solution to this problem is to assign a vertically independent lidar ratio to aerosol retrievals that fit a specific aerosol model as outlined in Omar et al. (2009).

To date, experimental techniques for directly measuring the lidar ratio include the use of high spectral resolution lidar (HSRL, Eloranta, 2005; Hair et al., 2008) and Raman lidar (RL, Ansmann et al., 1990). These instruments are capable of measuring aerosol backscatter and extinction parameters independently and therefore do not require the lidar ratio to be prescribed (e.g., Shipley et al., 1983; Grund and Eloranta, 1991; Piironen and Eloranta, 1994; Müller et al., 2007; Amiridis et al., 2009; Tesche et al., 2009a, b; Burton et al., 2012). On the other hand, Cattrall et al. (2005) use AERONET size distributions inverted from sun photometer data (Holben et al., 1998) to calculate the lidar ratio and then compare their indirect to literature reported direct measurements. They determined that their indirect method (285) compared well to the literature average of direct retrievals (295) (see Tables 3 and 4 in Cattrall et al., 2005). Direct measurements do not suffer the same limitations as indirect ones which require assumptions on size distribution and chemical composition or a molecular extinction profile. The Supplement Table S1 summarizes available retrieval methods and values of some experimentally determined lidar ratios over marine regions. Currently, most lidars do not yet have Raman or high spectral resolution capability and CALIPSO is the only lidar that provides aerosol data at the vast spatiotemporal resolution required for global climate model comparison.

Since the uncertainty in the lidar ratio can significantly affect the accuracy of the aerosol extinction retrieval (see a detailed discussion below), lidar ratios have been constrained by numerous approaches. However, marine aerosol size distribution, chemical composition and refractive index can change significantly with ocean surface wind speed ($U_{10}$), relative humidity (RH), temperature, salinity and chemical/biological composition of surface sea water (de Leeuw et al., 2011; Lewis and Schwartz, 2004). For this reason, large disagreement exists in the literature regarding the value of maritime aerosol lidar ratio ($S_p$; subscript "p" indicates particulate). For example, lidar measurements of Ansmann et al. (2001) over the North Atlantic showed $S_p = 24 \pm 5$ sr, whereas measurements using a nighttime lidar at a horizontal orientation off the northern coast of Queensland, Australia, showed maritime aerosol lidar ratios as high as $S_p = 39 \pm 5$ (Young et al., 1993). Using the data from AERONET oceanic sites, Cattrall et al. (2005) derived a lidar ratio of $28 \pm 5$ sr, a value that compared well with a literature averaged value of $S_p = 29 \pm 5$ sr (for $490 \leq \lambda \leq 550$ nm) for maritime aerosols. Passive techniques have also been used to derive the lidar ratio using an alternative definition of $S_p$ as a function of single scattering albedo and the scattering phase function near 180° (Bréon, 2013). Using the multi-directional measurements of solar radiation from the polarization sensitive passive radiometer POLDER, typical values for clean marine aerosol $S_p$ were derived to be 25 sr at 532 nm (Bréon, 2013). The lidar ratio of $20 \pm 6$ sr (at 532 nm) was selected for the CALIOP retrieval algorithm based on parameters measured during the Shoreline Environmental Aerosol Study (SEAS) experiment (Masonis et al., 2003; Omar et al., 2009). The SEAS measurements conducted on the beach (downwind of an offshore reef) report a particulate lidar ratio of $S_p = 25.4 \pm 3.5$ sr at 532 nm based on the optical size measurements of marine aerosol, and an average modeled value of $S_p = 20.3$ sr (Masonis et al., 2003). However, it was also shown that, depending on a particle size and wind speed regime, $S_p$ values can range from 10 to 90 sr (Masonis et al., 2003; Sayer et al., 2012). Therefore, as size distribution (and chemical composition) of marine aerosol may vary over the oceans, a constant lidar ratio used in CALIOP algorithms may lead to erroneous retrievals of AOD.

In this study, we present a new method for deriving lidar ratios for individual CALIOP retrievals of single aerosol layer columns over the ocean. We have used the Syner-

gized Optical Depth of Aerosols (SODA) product (described in Sect. 2.2) to estimate $S_p$ for a strictly defined subset of CALIPSO data. The $S_p$ values are calculated as a correction to achieve the best agreement between SODA and CALIPSO marine aerosol AOD values. Using CALIPSO level 2 aerosol layer data for years 2007 to 2010, we have created a 3-year averaged climatology of clean marine aerosol lidar ratio over the globe. Analyses were also carried out to assess dependence of $S_p$ values on wind speed and estimate possible error sources in our calculations.

## 2 Instrumentation and methods

### 2.1 CALIPSO satellite

The CALIPSO mission (Winker et al., 2009), launched on 28 April 2006, has been able to provide the scientific community with vertically resolved measurements of both aerosol and cloud optical properties like depolarization ratio (a measure of particle sphericity), AOD, and ice/water phase since June 2006. The CALIPSO payload includes a high-powered digital camera, an infrared radiometer, and the two-wavelength (532 and 1064 nm) near-nadir, polarization-sensitive elastic backscatter lidar CALIOP.

The level 1 data algorithms are responsible for the geolocation and range determination of the satellite and produce profiles of attenuated backscatter coefficients. Data in this work were obtained from the 5 km level 2 operational products, version 3.01. Level 2 products have undergone various processing algorithms from the Selective Iterated BoundarY Locator (SIBYL), the Scene Classification Algorithm (SCA), and the Hybrid Extinction Retrieval Algorithm (HERA) (Vaughan et al., 2004, 2009). First, SIBYL identifies layers, then the SCA identifies the type of feature (i.e., aerosol or cloud) and the subtype (i.e., aerosol type, ice/water phase), and finally the HERA generates extinction profiles for the feature. The theoretical basis of the algorithm can be found online at www-calipso.larc.nasa.gov/resources/project_documentation.php.

The CALIPSO 5 km aerosol layer data include many operational products, only a few of which are used in this study. Among them are the integrated attenuated backscatter and its uncertainty at 532 nm, the layer features such as number found in the column and their top and bottom altitudes, and the feature classification flags.

### 2.2 Synergized Optical Depth of Aerosols

CloudSat was launched in 2006 with CALIPSO and was positioned in sun-synchronous orbit as part of the A-Train satellite constellation. CloudSat and CALIPSO have paved the way for new multi-sensor data products like SODA to be developed. The main instrument on CloudSat is the Cloud Profiling Radar (CPR), a nearly nadir-looking (0.16°) 94 GHz ($\approx$ 3 mm; W-band) radar. The CPR, like CALIOP, can retrieve information on hydrometeor microphysical properties at different heights in a vertical column. The CPR signal is mostly attenuated by water vapor; however, for cloud-free regions over the ocean, the CPR data can be used to retrieve AOD. A method developed by Josset et al. (2008) and later expanded by Josset et al. (2010a) uses a combination of CALIOP and CPR measurements of the ocean surface reflectance to derive AOD. The design of SODA utilizes the ratio of the radar-to-lidar ocean surface scattering cross section to infer column optical depth for non-cloudy atmospheric columns. Since the radar signal attenuates mostly due to water vapor and the lidar signal weakens mostly due to aerosols, after the radar signal is corrected for attenuation by water vapor and oxygen, the change in the radar-to-lidar signal ratio is directly related to aerosol abundance (Josset et al., 2008, 2010a). Therefore, by using observations from two different sensors, SODA can eliminate uncertainties induced by the CALIOP aerosol extinction algorithm over oceans. SODA AODs have been shown to be in very good agreement with MODIS AOD retrievals (Josset et al., 2008). A more detailed description of the SODA technique and its application is given in Josset et al. (2008, 2010a, b, 2011, and 2012). The SODA products that are used in this study include the quality assurance measure "qa_flag_aerosol" and the 532 nm AOD.

### 2.3 Lidar ratio definition

One of the biggest advantages of the SODA product is that it removes the dependence of the prescribed lidar ratio while still utilizing the active sensors to retrieve an AOD, thereby providing a means for independent evaluation of the lidar ratio. In the current study we use Eq. (4) from Josset et al. (2011) to estimate lidar ratio from CloudSat/CALIOP measurements of AOD values. Following Fernald et al. (1972), the particulate two-way transmittance at height $Z$ can be written as

$$T^2(Z) = e^{-2S_p \int_0^Z \beta_p(z)\mathrm{d}z}, \quad (1)$$

where the lidar ratio at height $Z$ can be defined as the ratio of the particulate extinction to backscatter ($S_p = \frac{\sigma_p(Z)}{\beta_p(Z)}$). Differentiating Eq. (1) with respect to vertical coordinate ($z$) gives the particulate backscatter at height $Z$:

$$\beta_p(Z) = -\frac{1}{2S_p T^2(Z)} \frac{\mathrm{d}T^2(Z)}{\mathrm{d}Z}. \quad (2)$$

Since atmospheric constituents (molecules and different particle types) can interact with the lidar beam at different heights, the lidar ratio using remotely sensed data cannot be uniquely defined for a given atmospheric column. However, the lidar ratio is a particle intensive property (i.e., dependent on particle type and not on the amount). So, if we assume that there is only a single type of aerosol that is homogeneously distributed throughout the atmospheric column and that molecular scattering is sufficiently removed by the

CALIOP level 2 algorithms, then the column lidar ratio ($\overline{S_p}$) can be expressed as the ratio of the particulate column integrated extinction ($\overline{\tau_p}$ = AOD) to the attenuated backscatter ($\overline{\Gamma_p}$). Based on these assumptions, integration of Eq. (2) with respect to vertical coordinate gives the particulate lidar ratio as

$$\overline{S_p} = -\frac{\int_{T_p^2(0)}^{T_p^2(Z)} dT^2(z)}{\int_0^Z \beta_p(z) T_p^2(z) dz}. \quad (3)$$

If we first substitute in Eq. (3) the definition for two-way transmittance as $T_p^2 = e^{-2\overline{\tau_p}}$, then substitute the total particulate attenuated backscatter signal retrieved by the lidar as $\overline{\Gamma_p} = \int_0^Z \beta_p(z) T^2(z) dz$, and finally consider that $T_p^2(0) = 1$, the equation for a columnar particulate lidar ratio is

$$\overline{S_p} = \frac{1 - e^{-2\overline{\tau_p}}}{2\overline{\Gamma_p}}. \quad (4)$$

Equation (4) allows us to calculate marine aerosol lidar ratio from two independent sources: the AOD (i.e., $\overline{\tau_p}$) from SODA and the integrated attenuated backscatter ($\overline{\Gamma_p}$) from CALIOP. It should be noted that CALIOP estimation of $\overline{\Gamma_p}$ is difficult for layers that are not bounded by clear air (Vaughan et al., 2004) and therefore require carefully designed data screening algorithms. In Sect. 4 we carry out an error analysis to verify that uncertainties in $\overline{\Gamma_p}$ have a minimal effect on the retrieved lidar ratio.

### 2.4 Data selection method

As different aerosol sub-types have different lidar ratios, application of Eq. (4) to episodes when aerosols other than marine aerosols are present in the atmospheric column may lead to erroneous results for the calculated $\overline{S_p}$. We developed a strict scene selection algorithm to minimize the contamination of AOD and therefore $\overline{S_p}$ by aerosol types other than marine (e.g., anthropogenic pollution, biomass burning, and dust). The algorithm first uses the feature classification flags in the CALIOP aerosol layer product. We start with clean marine aerosol that is identified based on surface type (as determined by the location of the satellite) and then retain only the data with total integrated attenuated backscatter $\gamma' > 0.01\,km^{-1}\,sr^{-1}$ and volume depolarization ratio $\delta' < 0.05$. (Omar et al., 2009). As multiple types of aerosols can be found within retrieved vertical profiles (e.g., dust above marine aerosols), aerosol feature types that have been identified as marine in a given atmospheric column are not enough to carry out the analysis. Therefore, when determining the lidar ratio of marine aerosol using Eq. (4), the algorithm only retains the data in which clean marine is the only type of aerosol present in the entire cloud-free atmospheric column. To further reduce the uncertainty, we constrain the analysis to single layer profiles below 2 km and remove profiles in which marine aerosol layers are vertically stacked within an atmospheric column. Therefore, the vertically integrated particulate attenuated backscatter $\overline{\Gamma_p}$ is replaced by $\Gamma_p$. Similarly, the column lidar ratio $\overline{S_p}$ is reduced to $S_p$ in the remainder of the text. Note also that all quantities discussed are particulate quantities; therefore, molecular scattering is removed using gridded molecular and ozone number density profile data from the Goddard Earth Observing System Model, version 5 (GEOS-5), analysis product available from the NASA Global Modeling and Assimilation Office (GMAO) (Winker et al., 2009). Operationally, particulate scattering is determined to be where the ratio of the CALIOP 532 nm scattering profile normalized by the GEOS-5 molecular scattering profile is greater than one $\left(\frac{\beta'_{532}}{\beta_m} > 1\right)$. Errors associated with $\overline{\Gamma_p}$ are discussed in Sect. 4.

All data are for nighttime and are binned into $2^\circ \times 5^\circ$ (latitude and longitude, respectively) grid cells. Collocated wind speed is taken from the Advanced Microwave Scanning Radiometer – EOS (AMSR-E) observing system. To identify distinct features associated with the variability in marine aerosol lidar ratio over different parts of the oceans, the selected data are examined in relation with other variables such as season, spatial location, and wind speed.

Some additional measures were taken to target layers with a high signal-to-noise ratio and grid cells with a significant number of observations. These measures included (i) ensuring the relative error in $\Gamma_p$ due to random noise in molecular backscatter was $< 50\,\%$, (ii) the collocated SODA 5 km layer was composed of at least 70 % shot-to-shot data, and (iii) the total number of retrievals per $2^\circ \times 5^\circ$ grid cell ranked above the first quartile of the grid cell frequency distribution. Such strict quality controls considerably increase the reliability of the analysis despite reducing the total number of data points. It should be noted that a large number (over 260 000) of data points remained for robust statistics after all the quality control and quality assurance tests. A caveat, despite such rigorous quality control criteria, remains: when interpreting data near coastlines, the CALIOP scene classification algorithm may mistakenly identify mixtures of continental pollution and marine as clean marine aerosol (Burton et al., 2013; Oo and Holz, 2011; Schuster et al., 2012), causing an overestimation in the lidar ratio inferred from Eq. (4). Further discussion of error analysis is given in Sect. 4.

## 3 Results

### 3.1 Global distribution of retrieved AOD and lidar ratio

Active detectors like CALIOP require knowledge of the lidar ratio for retrieval of aerosol optical properties. Incorrect estimates of the $S_p$ values for a given aerosol type can lead to significant errors in the retrievals of particulate extinction and AOD. Past studies using collocated CALIOP and MODIS re-

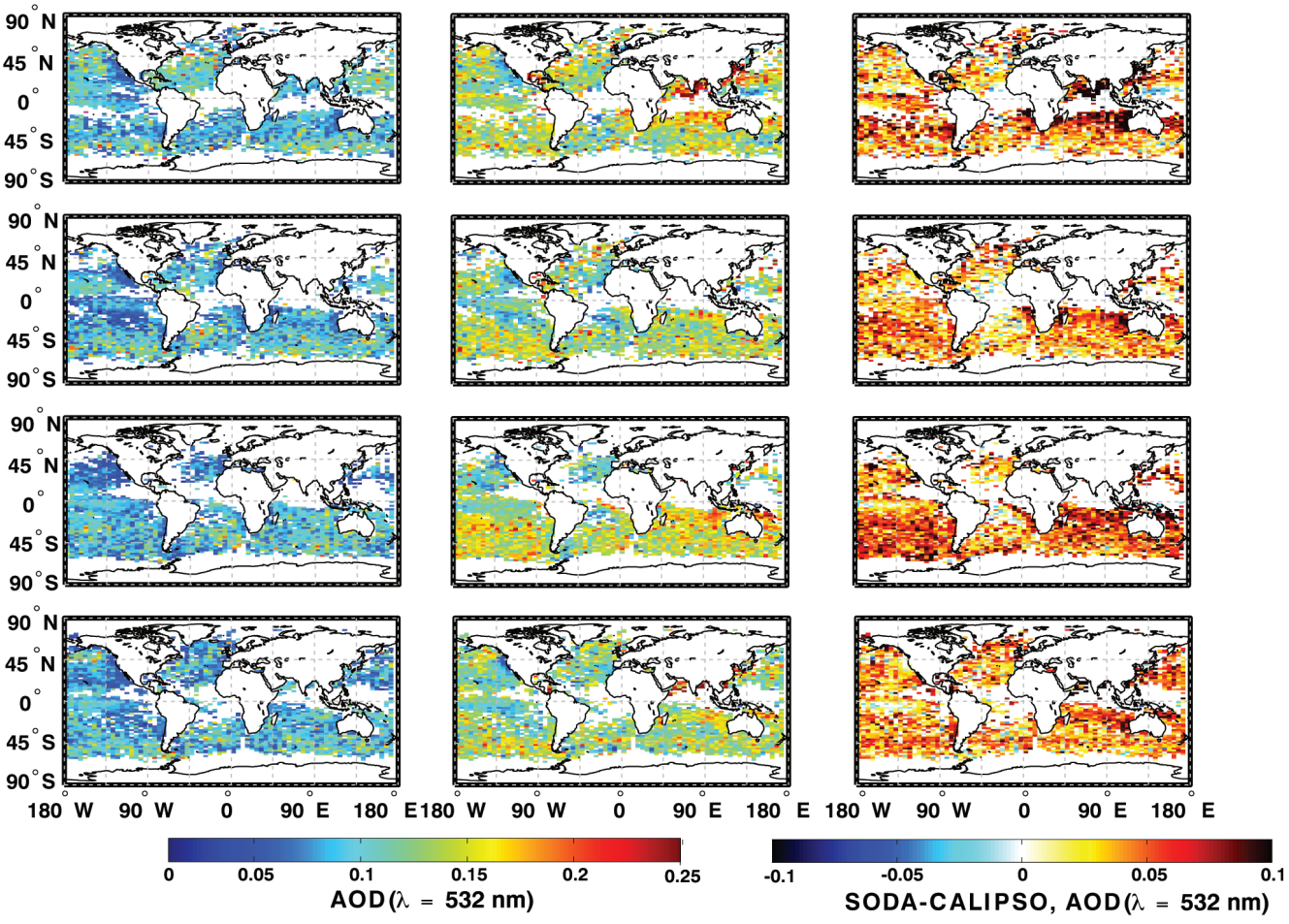


**Figure 1.** Seasonal median AOD values from CALIOP and SODA (columns 1 and 2) and the difference (SODA – CALIOP) plot (column 3) for December–February (row 1), March–May (row 2), June–August (row 3), and September–November (row 4) plotted on a 2° × 5° latitude longitude grid. "No data" areas are shaded white and defined as grid cells failing the quality-control algorithm (see text for details).

trievals have shown that, over the marine regions, CALIOP underestimates the AOD values relative to MODIS (Oo and Holz, 2011). As MODIS data over the ocean have been extensively evaluated with numerous field campaigns (e.g., Levy et al., 2005), it was suggested that the primary source of discrepancy between the two sensors was the low value of the marine aerosol lidar ratio used by CALIOP (Oo and Holz, 2011). Figure 1 shows seasonally averaged maps of CALIPSO and SODA marine aerosol median optical depth at 532 nm and the differences between SODA- and CALIOP-retrieved AODs. White regions in Fig. 1 represent grid cells that were rejected by the data selection algorithm and have been removed from the subsequent data analysis. Inspection of Fig. 1 reveals considerable spatial and temporal variations in marine aerosol AOD. Although the largest values of AOD seem to occur over regions with higher surface wind speed (i.e., the northern and southern oceans), elevated AOD values can also be seen over the regions downwind from dust and/or pollution sources such as the mid-latitude North Atlantic Ocean and the Bay of Bengal and over the major oceanic gyres. The region around the Indian subcontinent and over the Bay of Bengal is believed to be just a retrieval artifact. Large disagreements between SODA- and CALIOP-reported AODs for these regions suggest that some dust/pollution aerosols might have been misclassified by CALIOP as marine aerosol. Higher $S_p$ values for dust and pollution compared to marine aerosol would produce a higher AOD retrieval in SODA compared to CALIOP. Elevated AOD values over the oceanic regions with lower surface wind speed, however, could point to changes in marine aerosol size distribution to smaller sizes. Sub-micron sea salt aerosols (with particle diameter, $D_p < 1\,\mu m$) are believed to have larger lidar ratios than super-micron ones (e.g., Masonis et al., 2003; Oo and Holz, 2011). In general, Fig. 1 shows positive differences between SODA- and CALIOP-retrieved seasonal median AOD values. Recalling that CALIOP-retrieved extinction is the product of the prescribed lidar ratio and the measured column integrated particulate backscatter, positive

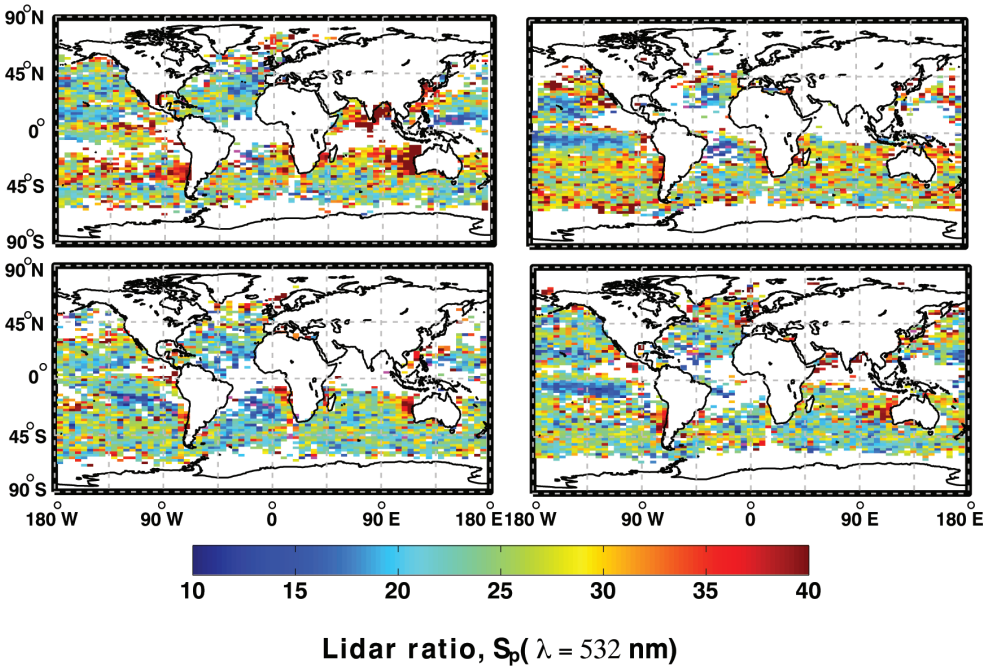


**Figure 2.** Seasonal lidar ratio for $2° \times 5°$ latitude longitude grid cells. Seasons are arranged as **(a)** December–February, **(b)** March–May, **(c)** June–August, **(d)** September–November.

differences between SODA and CALIOP median AODs at 532 nm over most of the oceans suggest underestimation of the marine aerosol lidar ratio prescribed in the CALIOP clean marine aerosol model. Figure 2 shows that over most of the ocean surfaces, the calculated lidar ratio is higher than the default ($S_p = 20$ sr) used in the CALIOP clean marine aerosol model. Global means and standard deviations for AOD and lidar ratio are given in Table 1. CALIOP retrievals in this study cannot be directly compared to MODIS since we only use nighttime data. Nevertheless, SODA retrievals of AOD have been shown to agree well with MODIS (Josset et al., 2008), HSRL (Fig. 7a; Josset et al., 2011) and Maritime Aerosol Network (MAN) (Smirnov et al., 2011; Fig. 8) observations, suggesting that the corrected lidar ratios will bring CALIOP retrievals close to MODIS data. Figure 2 also reveals that the value of the lidar ratio calculated using Eq. (4) changes considerably over different parts of the remote oceans, pointing to the variability in marine aerosol optical properties. It has long been known that meteorological and/or environmental factors and ocean chemical/biological composition influence marine aerosol production, entrainment, transport, and removal processes (Lewis and Schwartz, 2004) that can ultimately affect marine aerosol $S_p$. Moreover, due to atmospheric transport of marine aerosol, satellite-retrieved AOD values may also be related to the upwind processes. Despite the complexity of the mechanisms controlling marine aerosol mass concentration over the oceans, surface wind speed has always been considered as the major parameter governing the production, chemical composition, and life cycle of marine aerosol (Lewis and Schwartz, 2004). Therefore, in the next section we will investigate the effect of wind speed on calculated temporal variability of marine aerosol lidar ratio.

### 3.1.1 Wind speed dependence

Numerous investigators have examined the effect of sea surface wind speed and sea state on marine aerosol optical properties (e.g., Smirnov et al., 2003; Sayer et al., 2012). There are two mechanisms for primary marine aerosol production: bursting of bubbles at the water surface and mechanical tearing of water drops (spume) from wave crests (for surface wind speeds $U_{10} > 9\,\mathrm{m\,s^{-1}}$, Anguelova et al., 1999). Ocean bubbles are generated by the entrainment of air due to wave action. As bubbles rise due to their buoyancy they burst at the surface, producing marine aerosol. (Blanchard and Woodcock, 1957). In this study we have selected seven different wind speed regimes (see Table 2). The lowest wind speed regime, $0 < U_{10} \leq 4\,\mathrm{m\,s^{-1}}$, was chosen to represent aerosols not generated via wind driven processes over the ocean. In general, ocean waves break at wind speed values above $\sim 4\,\mathrm{ms^{-1}}$ (initiating the white cap formation and bursting of the entrained bubbles) (Lewis and Schwartz, 2004). Therefore, it has been suggested that below this threshold value, there should be a weak relationship between marine aerosol optical properties and the surface wind speed (Kiliyanpilakkil and Meskhidze, 2011; Lehahn et al., 2010). Moreover, for such a low wind speed regime, most of

**Table 1.** Seasonal means ± 1 standard deviations for 2° × 5° grid cell medians. The subscripts p, S, and C appended to $\tau$ stand for particulate, SODA, and CALIOP, respectively, where $\tau$ is the AOD.

| Season | $\tau_{p,S}$ | $\tau_{p,C}$ | $\Gamma_p \times 10^{-3}$ (sr$^{-1}$) | $S_p$ (sr) |
|---|---|---|---|---|
| Winter | $0.14 \pm 0.04$ | $0.09 \pm 0.03$ | $4.7 \pm 1.2$ | $27 \pm 8$ |
| Spring | $0.13 \pm 0.03$ | $0.09 \pm 0.03$ | $4.8 \pm 1.2$ | $24 \pm 7$ |
| Summer | $0.14 \pm 0.04$ | $0.09 \pm 0.03$ | $4.6 \pm 1.2$ | $27 \pm 8$ |
| Fall | $0.13 \pm 0.03$ | $0.09 \pm 0.03$ | $4.7 \pm 1.1$ | $25 \pm 7$ |

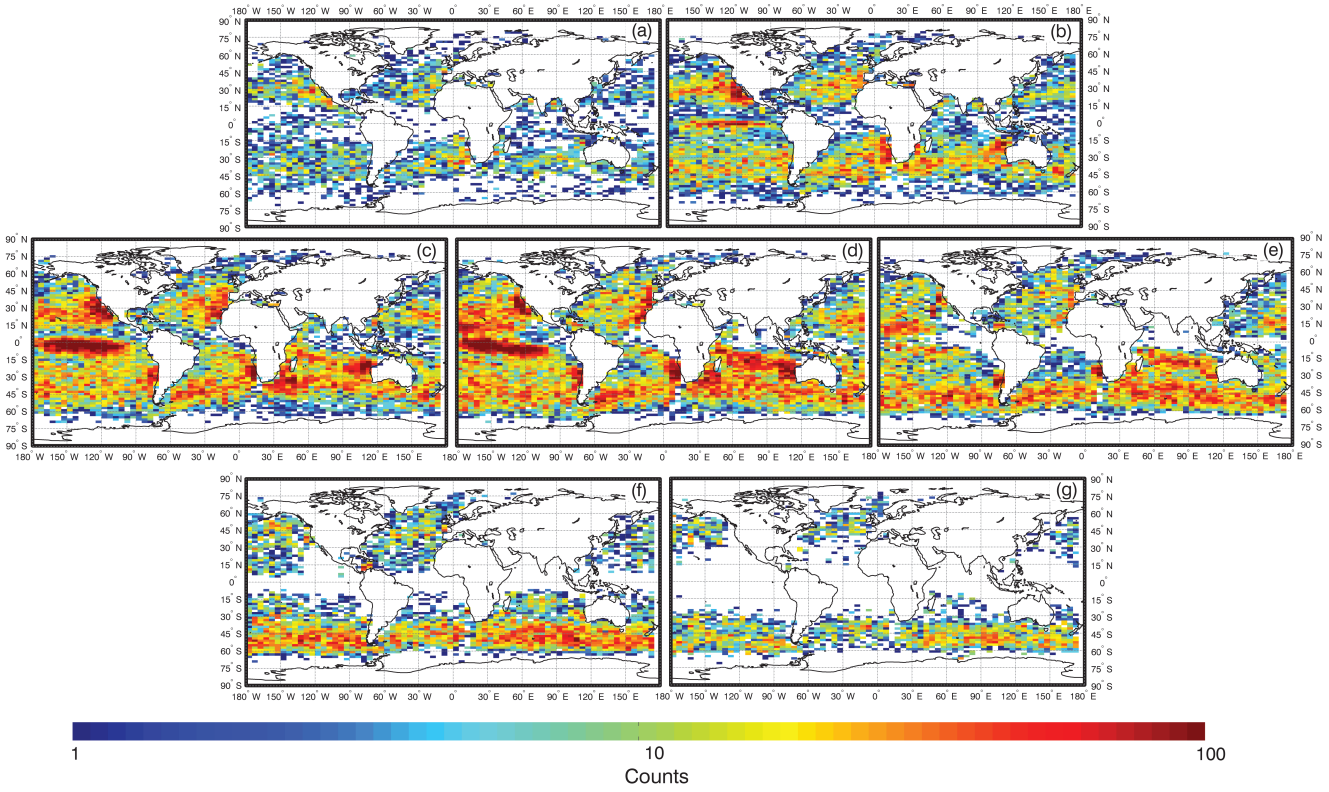


**Figure 3.** SODA/CALIOP retrieval counts for each 2° × 5° latitude longitude grid cell and different wind speed regimes. AMSR-E wind speed regimes for figures **(a)** through **(g)**, are 0–4, 4–6, 6–8, 8–10, 10–12, 12–15, and >15 m s$^{-1}$, respectively.

the aerosols classified as clean marine by CALIOP are either produced outside the swath and then blown into the satellite field of view or, like in cases near coastlines, mistakenly identified as marine aerosol. The highest wind speed regime, with $U_{10} > 15\,\mathrm{m\,s^{-1}}$, typically contributes a small fraction of CALIOP retrievals (Kiliyanpilakkil and Meskhidze, 2011) and is largely concentrated over the southern ocean and in the northern Atlantic where the highest wind speeds are observed (Bentamy et al., 2003). Figure 3 shows a spatial map of the number of retrievals for each grid cell separated by wind speed regime. According to Fig. 3, the southern ocean retrievals are dominant at the highest wind speeds and are overall consistent with the so-called "roaring forties" latitude band. Figure 3, as well as Table 2, shows that the fewest number of retrievals are found for the lowest and highest wind regimes.

The data shown in Fig. 3 are next used to generate scatter density plots for SODA- and CALIOP-retrieved AOD values for the wind speed regimes reported in Table 2 (see Fig. 4). As expected, Fig. 4 shows that increases in wind speed are typically associated with higher values of marine aerosol optical depth (note the center of the scatter distribution shifts slightly to higher AODs for larger wind speed values). However, as the majority of the SODA AODs exist above the 1 : 1 line, this figure also indicates the underestimation of CALIOP-retrieved marine aerosol optical depth values. When averaged over the entire globe, CALIOP-retrieved clean marine AOD is roughly 32 % lower compared to SODA (with an RMS error of 0.06; Supplement Fig. S2). Accord-

**Table 2.** Means ± 1 standard deviation for 2° × 5° grid cell medians for various AMSR-E wind speed regimes. The subscripts $p$, $S$ and $C$ appended to $\tau$ stand for particulate, SODA and CALIOP, respectively, where $\tau$ is the AOD.

| Wind regime ($ms^{-1}$) | $\tau_{p,S}$ | $\tau_{p,C}$ | $\Gamma_p \times 10^{-3}$ ($sr^{-1}$) | $S_p$ (sr) | Relative number(%) |
|---|---|---|---|---|---|
| $0 < U_{10} \leq 4$ | $0.12 \pm 0.05$ | $0.07 \pm 0.04$ | $3.6 \pm 1.4$ | $32 \pm 17$ | 11 849 (5) |
| $4 < U_{10} \leq 6$ | $0.11 \pm 0.04$ | $0.07 \pm 0.03$ | $3.8 \pm 1.1$ | $27 \pm 12$ | 32 899 (13) |
| $6 < U_{10} \leq 8$ | $0.12 \pm 0.04$ | $0.08 \pm 0.02$ | $4.2 \pm 1.0$ | $26 \pm 9$ | 60 083 (23) |
| $8 < U_{10} \leq 10$ | $0.13 \pm 0.03$ | $0.08 \pm 0.02$ | $4.7 \pm 1.0$ | $26 \pm 7$ | 68 899 (26) |
| $10 < U_{10} \leq 12$ | $0.15 \pm 0.04$ | $0.10 \pm 0.03$ | $5.1 \pm 1.0$ | $26 \pm 6$ | 45 895 (17) |
| $12 < U_{10} \leq 15$ | $0.16 \pm 0.04$ | $0.12 \pm 0.03$ | $5.7 \pm 1.2$ | $25 \pm 6$ | 30 162 (11) |
| $U_{10} > 15$ | $0.16 \pm 0.04$ | $0.14 \pm 0.04$ | $6.4 \pm 1.4$ | $22 \pm 7$ | 12 953 (5) |

ing to Fig. 4 the largest discrepancies between SODA and CALIOP retrievals are observed at lower wind speed values. One simple explanation for this is a greater chance for CALIOP misclassification over the oceanic regions where long-range continental aerosols can contribute a larger fraction of the marine boundary layer (MBL) particles (e.g., Blot et al., 2013). Terrestrial particles (e.g., mineral dust, anthropogenic pollution) are typically characterized by the larger lidar ratio values, leading to an underestimation of the CALIOP-retrieved AODs. However, measurements also show that changes in surface wind speed values can cause a considerable shift in the marine aerosol size distribution. For optically active marine aerosols, the residence time decreases considerably with increasing size. Thus the aerosol population is increasingly controlled by the smaller end of the particle size spectrum as wind speeds decrease over the ocean (Hoffman and Duce, 1974). Conversely, as wind speed increases, fine mode aerosol volume size distribution changes slightly (with mixed trends), while the coarse mode volume size distribution exhibits a large and positive response to the increase in wind speed (Lewis and Schwartz, 2004; Smirnov et al., 2003). Such variability in marine aerosol volume size distribution is expected to have an effect on the aerosol lidar ratio. As sub-micron marine aerosols are characterized with much larger lidar ratios than super-micron ones (e.g., Masonis et al., 2003; Oo and Holz, 2011), shifting marine aerosol size distribution spectra to smaller particles will cause an increase in total aerosol lidar ratio. Therefore for clean marine aerosols, AODs and lidar ratios are expected to have opposite dependences on wind speed: high wind speed regions are characteristic of high AODs and low lidar ratios while lower wind speeds favor higher lidar ratios and lower AODs (Smirnov et al., 2003; Sayer et al., 2012).

Figure 5 shows that on average, the calculated aerosol lidar ratio is weakly related to the surface wind speed. According to this figure, aerosols retrieved in the wind speed regime $0 < U_{10} \leq 4\,m\,s^{-1}$ depict the largest variability in the lidar ratio as indicated by the spread of the distribution. As discussed above, aerosols in this regime likely include both marine aerosols particles produced upwind and advected into the satellite field of view (with $S_p \sim 20$ to 30 sr)

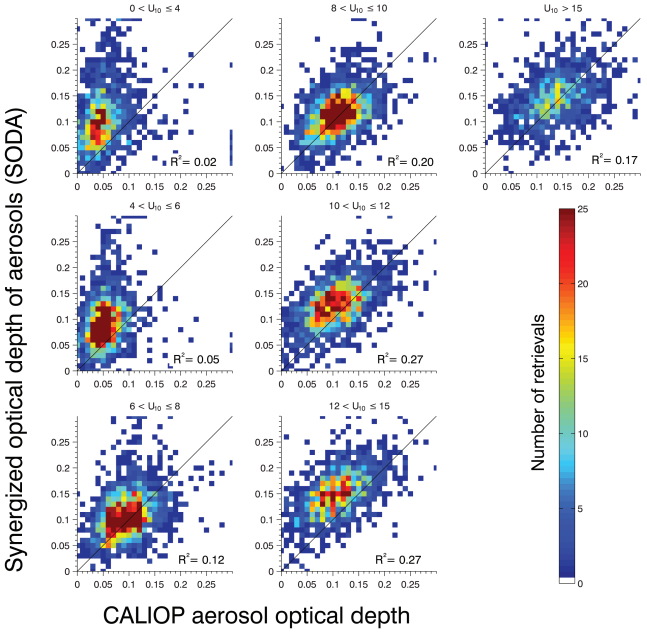


**Figure 4.** Scatter density plot of SODA to CALIOP AOD for each wind speed regime. Each point indicates a grid cell median, colored by frequency of occurrence. The black line is the 1 : 1 relationship, with reported $R^2$ values.

and dust/pollution particles (with $S_p \sim 40$ to 70 sr, Omar et al., 2009) that may have been misclassified by CALIOP as marine aerosol. As shown in Table 2, the marine aerosol lidar ratio distribution in this regime is characterized by the largest standard deviation ($\sigma = 17.4$ sr), indicating that for the lowest wind speed values, a wide range of marine aerosol sizes can be present over the ocean. Since the primary marine aerosol production is minimal for the wind speed values less than $4\,m\,s^{-1}$, such large spread could also indicate that under low wind conditions there is greater probability for natural continental and human-induced pollution aerosols to be miss-classified by CALIOP as clean marine.

For the higher wind speed values ($4 < U_{10} \leq 15\,m\,s^{-1}$), lidar ratio generally decreases with the increase in the wind speed and approaches the lidar ratios prescribed by CALIOP

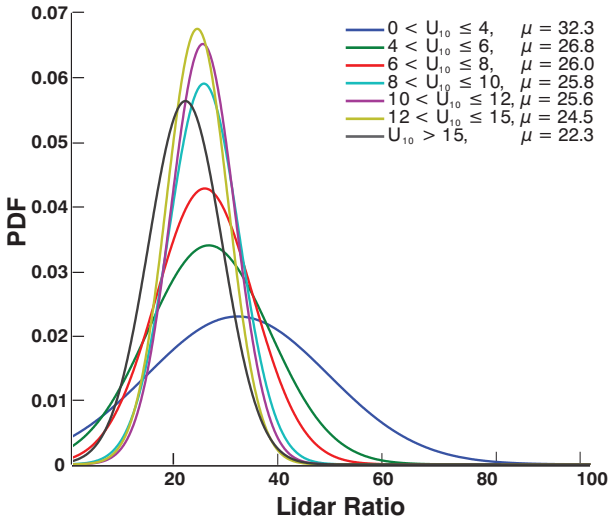


**Figure 5.** Probability density function of clean marine aerosol lidar ratio for selected AMSR-E wind speed regimes. The mean ($\mu$) of each distribution is also reported.

retrieval algorithms (i.e., 20 sr) at the highest wind speed regime. According to Table 2 and Fig. 3, the most common wind values in CALIOP marine aerosol retrievals over the ocean are in the $8 < U_{10} \leq 10\,\mathrm{m\,s^{-1}}$ regime (26 % of all available data) followed by the $6 < U_{10} \leq 8\,\mathrm{m\,s^{-1}}$ regime (23 % of all available data). For the higher wind speed regimes ($U_{10} > 6\,\mathrm{m\,s^{-1}}$), surface winds play a decisive role in the determination of the lidar ratio (indicated by the narrow standard deviation, see Table 2). This is an important result, as the distributions shown in Fig. 5 may help in providing additional criteria for clean marine lidar ratio selection, yielding improved retrievals of marine aerosol AOD from CALIOP.

Analysis of data indicates that a mean lidar ratio of 26 sr is the most probable value that occurs for the majority of CALIOP retrievals over the oceans. This value compares well with those reported in the literature. Müller et al. (2007) found a marine aerosol lidar ratio of $23 \pm 3$ and $23 \pm 5$ sr using RL, and Burton et al. (2012, 2013) reported a range from 15 to 27 sr using HSRL. Bréon (2013) used a different space-based retrieval and reported $S_\mathrm{p}$ for marine aerosol typically on the order of 25 sr. Table S1 reports some additional values of marine aerosol $S_\mathrm{p}$ measured by other techniques. This new lidar ratio reduces discrepancy between CALIOP-prescribed and SODA-derived lidar ratios from about 30 to 4 %.

Previous studies reported a small decrease in marine aerosol lidar ratio with the increase in wind speed (Sayer et al., 2012). In general, wind speed alone is expected to be a poor predictor of marine aerosol lidar ratio, as aerosol volume size distribution and optical properties are likely to be influenced by a number of other parameters including relative humidity and marine boundary layer depth. Furthermore, errors increase exponentially approaching the lowest optical depths and could be the reason for the large spread in the lidar ratio seen in Fig. 5. Untangling systematic error from real physical effects is difficult in the low (0–4 $\mathrm{m\,s^{-1}}$) wind speed regime and highlights the need for more accurate measurements for calm wind/low AOD conditions. Despite these complications, a shift to lower lidar ratios with increasing wind speed can be seen from Fig. 5 and warrants further investigation.

## 4 Uncertainties, errors, and sensitivity

The method used to derive the lidar ratio in this study depends on two parameters: the CALIOP-integrated attenuated particulate backscatter ($\Gamma_\mathrm{p}$) and the SODA aerosol optical depth ($\tau_\mathrm{p}$). Uncertainties in both $\Gamma_\mathrm{p}$ and $\tau_\mathrm{p}$ retrievals are expected to propagate through the calculations of the particulate lidar ratio. Josset et al. (2008, 2010a) investigate the domain of validity for $\tau_\mathrm{p}$ through an extensive calibration procedure. They find that for retrievals at wind speeds between 3 and 10 $\mathrm{ms^{-1}}$ the SODA product is in very good agreement ($R > 0.89$) with MODIS AOD, with calibration errors less than 15 %. Calibration errors in $\tau_\mathrm{p}$ are expected to be even lower for nighttime retrievals used in this study (Josset et al., 2008). However, average uncertainty for CALIOP $\Gamma_\mathrm{p}$ retrievals has not yet been examined and is necessary for the assessment of this retrieval method. We make an estimate on this uncertainty in the following section.

Since ocean is the source of marine aerosol, clean marine aerosol layers typically extend to the ocean surface. This makes it more difficult to determine molecular and particulate backscatter components of the signal separately using satellite measurements alone. To assess the uncertainty in lidar ratio introduced for the surface connected layers (i.e., layers whose bottom bound is defined as the ocean surface), we here estimate the error in CALIOP-retrieved $\Gamma_\mathrm{p}$ values. The total attenuated backscatter signal measured by the lidar consists of molecular and particulate components:

$$\beta_\mathrm{att} = (\beta_\mathrm{p} + \beta_\mathrm{m}) e^{-2\tau_\mathrm{p}} \cdot e^{-2\tau_\mathrm{m}}, \tag{5}$$

with subscripts $m$ and $p$ representing molecular and particulate quantities, respectively. From the definition of $\Gamma_\mathrm{p}$ it follows that

$$\Gamma_\mathrm{p} = \int_0^Z \beta_\mathrm{p}(z) e^{-2\tau_\mathrm{p}} \mathrm{d}z, \tag{6}$$

where the integration is from the surface to the top of the layer. $\beta_\mathrm{p}$ is the particulate backscatter and $e^{-2\tau_\mathrm{p}}$ accounts for the attenuation of the lidar signal by the particles. Substituting Eq. (5) into Eq. (6) gives

$$\Gamma_\mathrm{p} = \int_0^Z (\beta_\mathrm{att} e^{2\tau_\mathrm{m}} - \beta_\mathrm{m}(z) e^{-2\tau_\mathrm{p}}) \mathrm{d}z. \tag{7}$$

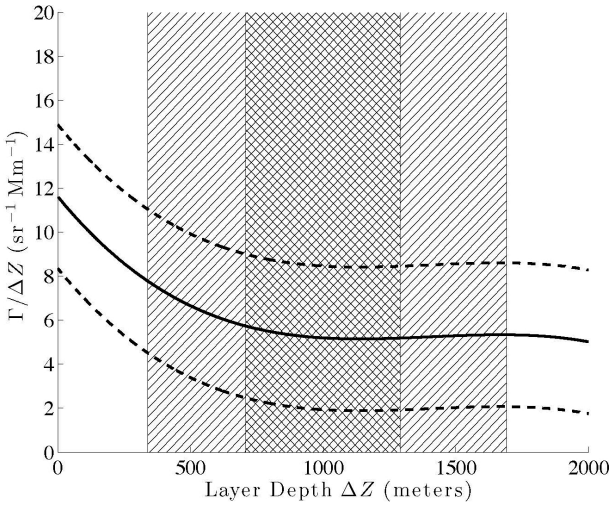


**Figure 6.** The normalized integrated attenuated backscatter as a function of the layer depth. The solid line shows the third-order least squares fit to the data while the dotted lines show $\pm 1\sigma$; the hatched area shows the layer depth data frequency: cross hatch between the 25th and 75th percentiles and straight hatch between 5th and 95th percentiles.

The molecular component of the signal in Eq. (7) can be derived from the GMAO modeled temperature and pressure profiles (Bloom et al., 2005). However, to solve this equation and determine the particulate attenuated backscatter value, particulate column-integrated extinction is required. To get $\tau_p$, the CALIOP algorithm uses a prescribed value of the lidar ratio, making Eq. (4) circularly dependent. The error in CALIOP-retrieved $\Gamma_p$ associated with the prescribed lidar ratio can be estimated by substituting the $\tau_p$ value from SODA. A large error would imply that the uncertainty in CALIOP-prescribed lidar ratio would introduce sizable corrections to $\Gamma_p$, making Eq. (4) unsuitable for the estimation of marine aerosol lidar ratio.

The relative error in $\Gamma_p$ can be defined as

$$\text{Error} = \frac{\Gamma_{p,S} - \Gamma_{p,C}}{\Gamma_{p,C}} = \frac{(e^{-2\tau_{p,C}} - e^{-2\tau_{p,S}}) \cdot \int_0^Z \beta_m(z)\mathrm{d}z}{\Gamma_{p,C}}, \quad (8)$$

where $\Gamma_{p,S}$ and $\Gamma_{p,C}$ are columnar integrated attenuated backscatter values for SODA and CALIOP, respectively. From the theoretical basis documents for CALIOP level 1 algorithms, the molecular backscatter is estimated as $\beta_m = \frac{C_s}{S_m}\frac{T(z)}{P(z)}$, where height-dependent $T(z)$ and $P(z)$ profiles from the surface (1000 hPa) to top-of-atmosphere (0.1 hPa) pressure levels were obtained from the GMAO Modern-Era Retrospective analysis for Research and Applications data set. The molecular lidar ratio, $S_m$, is defined as $8\pi/3$, and $C_s$ is a constant equal to $3.742 \times 10^{-6}$ K hPa$^{-1}$ m$^{-1}$ (Hostetler et al., 2005). When considering all of the parameters, our analysis shows that the average error in $\Gamma_p$ is approximately 1.5 %. Compared to the systematic uncertainty in the SODA product < 15%, the uncertainty in $\Gamma_p$ is much lower, indicating that, on average, errors in $\Gamma_p$ do not dominate $S_p$ retrievals. Since an average discrepancy between CALIOP-prescribed and SODA-derived lidar ratios ($\sim$ 30 %) is more than an order of magnitude higher than uncertainty in $\Gamma_p$, we conclude that the uncertainty in the CALIOP column-integrated backscatter has a minor effect on the Eq. (4) calculated lidar ratio.

Furthermore, because in our study we use feature-integrated products for a single aerosol layer, it is also important to evaluate the relationship between $\Gamma_p$ and aerosol layer thickness ($\Delta Z$). Figure 6 shows the normalized column attenuated particulate backscatter $\Gamma_p$ as a function of layer depth. For uniformly distributed aerosols throughout the column, $\Gamma_p$ is likely to be proportional to $\Delta Z$. The spread of $\Gamma_p/\Delta Z$ ratio is indicative of different amounts of marine aerosol present in the column. Two limits of very high and very low $\Delta Z$ values are of particular interest. For example, strong reduction of the $\Gamma_p/\Delta Z$ ratio at the higher $\Delta Z$ values would indicate that the lidar signal is strongly attenuated throughout the layer reaching a sensitivity limit. However, considerable increase of the ratio for the thin layers may indicate contamination of the backscattered signal by strong surface reflectance. According to Fig. 6, for the vast majority of the data, signal attenuation and surface reflectance do not seem to be major issues for the surface connected layers, suggesting that the quality control algorithm described in Sect. 2.4 was sufficient to remove the majority of erroneous measures of $\Gamma_p$.

To further assess the reliability of SODA marine aerosol product we also compared collocated HSRL (Fig. 7) and MAN (Fig. 8) AODs to SODA. Figure 7a shows results from three CALIPSO (and therefore SODA) underflights validated against HSRL. According to Fig. 7a for AODs < 0.3 (comprising the majority of marine aerosol retrievals), SODA compares reasonably well to HSRL ($R^2 = 0.82$, RMSE = 0.04; similar to the MAN comparison with RMSE = 0.03 in Fig. 8). Additionally, Fig. 7b illustrates that the relative uncertainty in the SODA-retrieved $S_p$ is typically below 50 % for AODs > 0.05. In our study, the bulk of AODs measured by SODA (98 %) exceed this value under the quality control criteria discussed in Sect. 2.4. Errors were estimated based on Eq. (15) in Josset et al. (2012), and for AODs > 0.05 we expect lidar ratio retrieval uncertainties below 50 %. MAN and SODA collocation for Fig. 8 was determined based on a scheme in Smirnov et al. (2011) and Kleidman et al. (2011). We required that the SODA retrieval be within $\pm$ 30 min of the MAN retrieval as well as within a circle with radius of 25 km around the MAN measurement. A map of the retrieval locations and the details of the algorithm used are given in the Supplement (Fig. S1). There were 51 matching MAN data points that passed the collocation screening. The MAN data corresponding to the same SODA retrieval were averaged and used to generate the scatter plot of MAN and SODA comparison (Fig. 8). The error

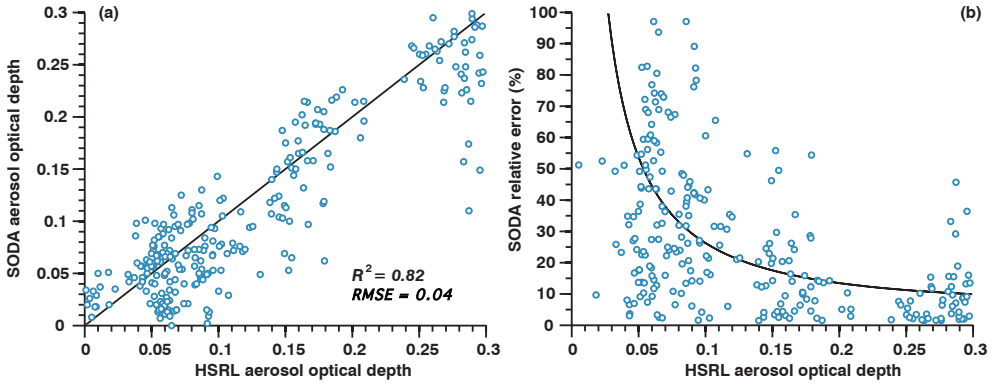


**Figure 7. (a)** A scatter plot of SODA AOD relative to AOD measured by HSRL at 532 nm with corresponding $R^2$ and RMSE. The black line illustrates the 1 : 1 line. **(b)** Relative uncertainty in the SODA column lidar ratio as a function of HSRL AOD with the black line showing the least squares exponential fit as in Josset et al. (2012), Eq. (15). All points are classified as marine plus pollution or marine plus dust and are from Table 1 in Josset et al. (2011).

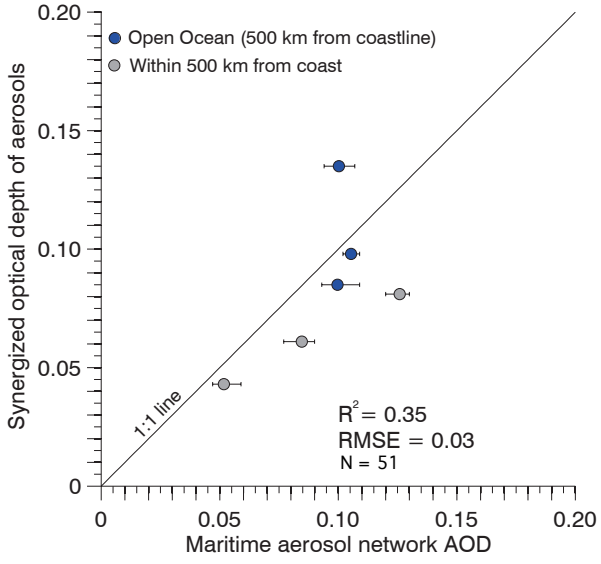


**Figure 8.** Scatter plot comparing the aerosol optical depth from SODA ($y$ axis) and AERONET Maritime Aerosol Network ($x$ axis). Blue circles represent locations that are at least 500 km from a coastline and are considered to be "open ocean".

bars in Fig. 8 indicate the maximum and minimum values of the MAN AOD reported for the closest SODA retrieval. Figure 8 shows that in general there is a good agreement between SODA and MAN retrievals with the data points located reasonably close to the 1 : 1 line. The correlation is 0.59 and the RMS error is 0.03.

## 5 Conclusions

A new method showing that it is possible to infer lidar ratios of marine aerosol over the ocean using two independent sources: the AOD from Synergized Optical Depth of Aerosols and the integrated attenuated backscatter from Cloud-Aerosol Lidar with Orthogonal Polarization has here been applied. The proposed equation calculates particulate lidar ratio for individual CALIOP retrievals of single aerosol layer columns as a correction to achieve the best agreement between SODA and CALIOP retrievals. The new method allows calculating marine aerosol lidar ratio and assessing its spatiotemporal variability and dependence on ocean surface wind speed. Analyses were carried out using CALIOP level 2, 5 km aerosol layer and collocated SODA nighttime data from December 2007 to November 2010. During the data analysis, over 260 000 data points passed various quality-control and quality-assurance tests to reduce errors associated with the clean marine aerosol retrievals. The calculated lidar ratios have been analyzed over the global ocean, covering a wide range of wind speed and AOD conditions. Data analysis shows that over most of the ocean surfaces, the calculated lidar ratio is higher than the default lidar ratio of 20 sr used in the CALIOP clean marine aerosol model. The calculated aerosol lidar ratios are inversely related to the surface wind speed. Increases in mean surface ocean wind speeds from 0 to $>15\,\mathrm{ms}^{-1}$ reduces the mean lidar ratio for marine aerosol from $\sim 32$ sr to $\sim 22$ sr. Such reduction was explained by the shift in aerosol volume size distribution with the wind speed; however, it was also emphasized that future studies should explore the role of meteorological and/or environmental factors and ocean chemical/biological composition for marine aerosol intensive properties. Our data analysis showed that changes in wind speed also affect the probability density function for marine aerosol lidar ratio distribution. The largest standard deviation calculated for the lowest wind

speed regime suggested that under low wind conditions, a wide range of marine aerosol sizes can be present over the ocean and there is greater probability for natural-continental and human-induced pollution aerosols to be classified by CALIOP as clean marine. We would like to mention that the role of organic aerosol at low wind speeds is still unclear. A large body of experimental data suggests that increases in the organic fraction of marine aerosol can have implications on hygroscopicity (e.g., Saxena et al., 1995; Fuentes et al., 2011; Ovadenevaite et al., 2013) and could potentially influence our results. Overall, our data analysis shows that an average value of 26 sr for clean marine aerosol lidar ratio provides the best agreement between the SODA product and CALIOP-retrieved global mean marine aerosol optical depth values. However, our study also shows large spatiotemporal variability in marine aerosol lidar ratios, suggesting that a single constant value of the lidar ratio is not suitable for a wide range of marine aerosol and can lead to large uncertainties at different locations and seasons.

We have estimated the error in CALIOP-retrieved column integrated attenuated particulate backscatter. Calculations suggest that the average uncertainty in particulate backscatter is more than an order of magnitude lower compared to the retrieved value. Data analysis also showed no clear indication for either approaching a sensitivity limit (due to strong attenuation of the lidar signal throughout the layer) or the contamination of the backscattered signal by the surface reflectance. Based on the conducted error analysis we conclude that the strict quality control criteria developed in this study is adequate to remove the majority of erroneous retrievals.

Finally, even though calculations here were carried out for marine aerosol, the technique used in this study is broad and can be used to infer lidar ratios of different species of atmospheric aerosols (i.e., mineral dust, biomass burning, etc.) advecting over the ocean. Because our data analysis shows that it is possible to derive a correction to the CALIOP prescribed marine aerosol lidar ratio, future studies should also consider conducting case studies over different oceanic regions to examine the possible effects of meteorological parameters and ocean physiochemical/biological composition on marine aerosol lidar ratio. Classification of the spatiotemporal distribution and wind speed dependence of a limited number of parameters affecting marine aerosol lidar ratios may lead to improved retrievals of AOD values over the oceans.

**The Supplement related to this article is available online at doi:10.5194/acp-15-3241-2015-supplement.**

*Acknowledgements.* This research was supported by the National Aeronautics and Space Administration (NASA) through grant numbers NNX11AG72G and NNX14AL89G and by the National Science Foundation through the grant AGS-1249273. The authors gratefully acknowledge the CALIPSO, CloudSat, and NASA Langley HSRL Teams for their support and effort in making the data available. CALIPSO data were obtained from the NASA Langley Research Center Atmospheric Science Data Center. CloudSat data are produced by remote sensing systems and sponsored by the NASA Earth Science MEaSUREs DISCOVER Project and the Advanced Microwave Scanning Radiometer (AMSR-E) Science Team. The SODA product is developed at the ICARE data and services center (http://www.icare.univ-lille1.fr) in Lille (France) in the frame of the CALIPSO mission and supported by CNES.

Edited by: C. McNeil

## References

Ackermann, J.: The extinction-to-backscatter ratio of tropospheric aerosol: A numerical study, J. Atmos. Ocean. Technol., 15, 1043–1050, doi:10.1175/1520-0426(1998)015<1043:TETBRO>2.0.CO;2, 1998.

Amiridis, V., Balis, D. S., Giannakaki, E., Stohl, A., Kazadzis, S., Koukouli, M. E. and Zanis, P.: Optical characteristics of biomass burning aerosols over Southeastern Europe determined from UV-Raman lidar measurements, Atmos. Chem. and Phys., 9, 2431–2440, doi:10.5194/acp-9-2431-2009, 2009.

Andreae, M. O.: Aerosols before Pollution, Science, 315, 50–51, 10.2307/20035138, 2007.

Anguelova, M., Barber Jr, R. P., and Wu, J.: Spume drops produced by the wind tearing of wave crests, J. Phys. Oceanogr., 29, 1156–1165, doi:10.1175/1520-0485(1999)029<1156:SDPBTW>2.0.CO;2, 1999.

Ansmann, A., Riebesell, M., and Weitkamp, C.: Measurement of atmospheric aerosol extinction profiles with a Raman lidar, Opt. Lett., 15, 746–748, doi:10.1364/OL.15.000746, 1990.

Ansmann, A., Wagner, F., Althausen, D., Müller, D., Herber, A., and Wandinger, U.: European pollution outbreaks during ACE 2: Lofted aerosol plumes observed with Raman lidar at the Portuguese coast, J. Geophys. Res., 106, 20725–20733, doi:10.1029/2000JD000091, 2001.

Ansmann, A. and Múller, D.: Lidar and Atmospheric Aerosol Particles, in: Lidar, edited by: Weitkamp, C., Springer New York, 105–141, 2005.

Bentamy, A., Katsaros, K. B., Mestas-Nuñez, A. M., Drennan, W. M., Forde, E. B., and Roquet, H.: Satellite estimates of wind speed and latent heat flux over the global oceans, J. Climate, 16, 637–656, doi:10.1175/1520-0442(2003)016<0637:SEOWSA>2.0.CO;2, 2003.

Blanchard, D. and Woodcock, A.: Bubble formation and modification in the sea and its meteorological significance, Tellus, 9, 145–158, doi: 10.1111/j.2153-3490.1957.tb01867.x, 1957.

Bloom, S., Da Silva, A., Dee, D., Bosilovich, M., Chern, J., Pawson, S., Schubert, S., Sienkiewicz, M., Stajner, I., and Tan, W.: Documentation and validation of the Goddard Earth Observing System (GEOS) data assimilation system – Version 4, NASA Tech. Memo., 104606, 187, 2005.

Blot, R., Clarke, A. D., Freitag, S., Kapustin, V., Howell, S. G., Jensen, J. B., Shank, L. M., McNaughton, C. S., and Brekhovskikh, V.: Ultrafine sea spray aerosol over the southeast-

ern Pacific: open-ocean contributions to marine boundary layer CCN, Atmos. Chem. Phys., 13, 7263–7278, doi:10.5194/acp-13-7263-2013, 2013.

Bréon, F. M.: Aerosol extinction-to-backscatter ratio derived from passive satellite measurements, Atmos. Chem. Phys., 13, 8947–8954, doi:10.5194/acp-13-8947-2013, 2013.

Burton, S., Ferrare, R., Hostetler, C., Hair, J., Rogers, R., Obland, M., Butler, C., Cook, A., Harper, D., and Froyd, K.: Aerosol classification using airborne High Spectral Resolution Lidar measurements–methodology and examples, Atmos. Meas. Tech., 5, 73–98, doi:10.5194/amtd-4-5631-2011, 2012.

Burton, S. P., Ferrare, R. A., Vaughan, M. A., Omar, A. H., Rogers, R. R., Hostetler, C. A., and Hair, J. W.: Aerosol classification from airborne HSRL and comparisons with the CALIPSO vertical feature mask, Atmos. Meas. Tech., 6, 1397–1412, doi:10.5194/amt-6-1397-2013, 2013.

Carslaw, K. S., Lee, L. A., Reddington, C. L., Pringle, K. J., Rap, A., Forster, P. M., Mann, G. W., Spracklen, D. V., Woodhouse, M. T., Regayre, L. A., and Pierce, J. R.: Large contribution of natural aerosols to uncertainty in indirect forcing, Nature, 503, 67, doi:10.1038/nature12674, 2013.

Cattrall, C., Reagan, J., Thome, K., and Dubovik, O.: Variability of aerosol and spectral lidar and backscatter and extinction ratios of key aerosol types derived from selected Aerosol Robotic Network locations, J. Geophys. Res., 110, D10S11, doi:10.1029/2004JD005124, 2005.

de Leeuw, G., Andreas, E. L., Anguelova, M. D., Fairall, C., Lewis, E. R., O'Dowd, C., Schulz, M., and Schwartz, S. E.: Production flux of sea spray aerosol, Rev. Geophys., 49, doi:10.1029/2010RG000349, 2011.

Doherty, S. J., Anderson, T. L., and Charlson, R. J.: Measurement of the lidar ratio for atmospheric aerosols with a 180 backscatter nephelometer, Appl. Opt., 38, 1823–1832, 1999.

Eloranta, E.: High spectral resolution lidar, in: Lidar: Range-Resolved Optical Remote Sensing of the Atmosphere, edited by: Weitkamp, K., Springer, New York, 143–163, 2005.

Fernald, F. G., Herman, B. M., and Reagan, J. A.: Determination of aerosol height distributions by lidar, J. Appl. Meteorol., 11, 482–489, 1972.

Fuentes, E., Coe, H., Green, D., and McFiggans, G.: On the impacts of phytoplankton-derived organic matter on the properties of the primary marine aerosol – Part 2: Composition, hygroscopicity and cloud condensation activity, Atmos. Chem. Phys., 11, 2585–2602, doi:10.5194/acp-11-2585-2011, 2011.

Ghan, S., Laulainen, N., Easter, R., Wagener, R., Nemesure, S., Chapman, E., Zhang, Y., and Leung, R.: Evaluation of aerosol direct radiative forcing in MIRAGE, J. Geophys. Res., 106, 5295–5316, doi:10.1029/2000JD900502, 2001.

Groß S., Esselborn, M., Weinzierl, B., Wirth, M., Fix, A., and Petzold, A.: Aerosol classification by airborne high spectral resolution lidar observations, Atmos. Chem. Phys., 13, 2487–2505, doi:10.5194/acp-13-2487-2013, 2013.

Groß, S., Gasteiger, J., Freudenthaler, V., Wiegner, M., Geiß, A., Schladitz, A., Toledano, C., Kandler, K., Tesche, M., Ansmann, A., and Wiedensohler, A.: Characterization of the planetary boundary layer during SAMUM-2 by means of lidar measurements, Tellus B, 63, 695–705, doi:10.1111/j.1600-0889.2011.00557.x, 2011a.

Groß S., Tesche, M., Voker, F., Toledano, C., Wiegner, M., Ansmann, A., Althausen, D., and Seefeldner, M.: Characterization of Saharan dust, marine aerosols and mixtures of biomass-burning aerosols and dust by means of multi-wavelength depolarization and Raman lidar measurements during SAMUM 2, Tellus B, 63, 706–724, doi:10.1111/j.1600-0889.2011.00556.x, 2011b.

Grund, C. J. and Eloranta, E. W.: University of Wisconsin High Spectral Resolution Lidar, Optical Engineering, 30, 6–12, doi:10.1117/12.55766, 1991.

Hair, J. W., Hostetler, C. A., Cook, A. L., Harper, D. B., Ferrare, R. A., Mack, T. L., Welch, W., Izquierdo, L. R., and Hovis, F. E.: Airborne High Spectral Resolution Lidar for profiling aerosol optical properties, Appl. Opt., 47, 6734–6752, doi:10.1364/AO.47.006734, 2008.

Hoffman, E. J. and Duce, R. A.: The organic carbon content of marine aerosols collected on Bermuda, J. Geophys. Res., 79, 4474–4477, 1974.

Holben, B. N., Eck, T. F., Slutsker, I., Tanré, D., Buis, J. P., Setzer, A., Vermote, E., Reagan, J. A., Kaufman, Y. J., Nakajima, T., Lavenu, F., Jankowiak, I., and Smirnov, A.: AERONET-A Federated Instrument Network and Data Archive for Aerosol Characterization, Remote Sens. Environ., 66, 1, doi:10.1016/S0034-4257(98)00031-5, 1998.

Hoose, C., Kristjánsson, J., Iversen, T., Kirkevåg, A., Seland, Ø., and Gettelman, A.: Constraining cloud droplet number concentration in GCMs suppresses the aerosol indirect effect, Geophys. Res. Lett., 36, L12807, doi:10.1029/2009GL038568, 2009.

Hostetler, C., Liu, Z., Reagan, J., Vaughan, M., Winker, D., Osborn, M., Hunt, W., Powell, K., and Trepte, C.: CALIOP algorithm theoretical basis document – Part 1: Lidar level I ATBD-Calibration and level 1 data products, Rep.PC-SCI, 201, 66, 2005.

Josset, D., Pelon, J., Protat, A., and Flamant, C.: New approach to determine aerosol optical depth from combined CALIPSO and CloudSat ocean surface echoes, Geophys. Res. Lett., 35, L10805, doi:10.1029/2008GL033442, 2008.

Josset, D., Pelon, J., and Hu, Y.: Multi-instrument calibration method based on a multiwavelength ocean surface model, Geoscience and Remote Sensing Letters, IEEE, 7, 195–199, doi:10.1109/LGRS.2009.2030906, 2010a.

Josset, D., Zhai, P., Hu, Y., Pelon, J., and Lucker, P. L.: Lidar equation for ocean surface and subsurface, Opt. Express, 18, 20862–20875, doi:10.1364/OE.18.020862, 2010b.

Josset, D., Rogers, R., Pelon, J., Hu, Y., Liu, Z., Omar, A., and Zhai, P.: CALIPSO lidar ratio retrieval over the ocean, Opt. Express, 19, 18696–18706, doi:10.1364/OE.19.018696, 2011.

Josset, D., Pelon, J., Garnier, A., Hu, Y., Vaughan, M., Zhai, P., Kuehn, R., and Lucker, P.: Cirrus optical depth and lidar ratio retrieval from combined CALIPSO-CloudSat observations using ocean surface echo, J. Geophys. Res., 117, D05207, doi:10.1029/2011JD016959, 2012.

Kaufman, Y. J., Tanré, D., and Boucher, O.: A satellite view of aerosols in the climate system, Nature, 419, 215–223, doi:10.1038/nature01091, 2002.

Kiliyanpilakkil, V. P. and Meskhidze, N.: Deriving the effect of wind speed on clean marine aerosol optical properties using the A-Train satellites, Atmos. Chem. Phys., 11, 11401–11413, doi:10.5194/acp-11-11401-2011, 2011.

Kleidman, R. G., Smirnov, A., Levy, R. C., Mattoo, S., and Tanre, D.: Evaluation and Wind Speed Dependence of MODIS Aerosol

Retrievals Over Open Ocean, IEEE T. Geosci. Remote, 99, 1–7, doi:10.1109/TGRS.2011.2162073, 2011.

Lehahn, Y., Koren, I., Boss, E., Ben-Ami, Y., and Altaratz, O.: Estimating the maritime component of aerosol optical depth and its dependency on surface wind speed using satellite data, Atmos. Chem. Phys., 10, 6711–6720, doi:10.5194/acp-10-6711-2010, 2010.

Levy, R., Remer, L., Martins, J., Kaufman, Y., Plana-Fattori, A., Redemann, J., and Wenny, B.: Evaluation of the MODIS aerosol retrievals over ocean and land during CLAMS, J. Atmos. Sci., 62, 974–992, doi:10.1175/JAS3391.1, 2005.

Lewis, R. and Schwartz, E.: Sea salt aerosol production: mechanisms, methods, measurements and models – a critical review, American Geophysical Union, doi:10.1029/GM152, 2004.

Masonis, S. J., Anderson, T. L., Covert, D. S., Kapustin, V., Clarke, A. D., Howell, S., and Moore, K.: A Study of the Extinction-to-Backscatter Ratio of Marine Aerosol during the Shoreline Environment Aerosol Study, J. Atmos. Ocean. Technol., 20, 1388–1402, doi:10.1175/1520-0426(2003)020<1388:ASOTER>2.0.CO;2, 2003.

Meskhidze, N., Xu, J., Gantt, B., Zhang, Y., Nenes, A., Ghan, S., Liu, X., Easter, R., and Zaveri, R.: Global distribution and climate forcing of marine organic aerosol – Part 1: Model improvements and evaluation, Atmos. Chem. Phys., 11, 11689–11705, doi:10.5194/acp-11-11689-2011, 2011.

Müller, D., Ansmann, A., Mattis, I., Tesche, M., Wandinger, U., Althausen, D., and Pisani, G.: Aerosol-type-dependent lidar ratios observed with Raman lidar, J. Geophys. Res., 112, doi:10.1029/2006JD008292, 2007.

Omar, A. H., Winker, D. M., Kittaka, C., Vaughan, M. A., Liu, Z., Hu, Y., Trepte, C. R., Rogers, R. R., Ferrare, R. A., Lee, K., Kuehn, R. E., and Hostetler, C. A.: The CALIPSO Automated Aerosol Classification and Lidar Ratio Selection Algorithm, J. Atmos. Ocean. Technol., 26, 1994–2014, doi:10.1175/2009JTECHA1231.1, 2009.

Oo, M. and Holz, R.: Improving the CALIOP aerosol optical depth using combined MODIS-CALIOP observations and CALIOP integrated attenuated total color ratio, J. Geophys. Res., 116, D14201, doi:10.1029/2010JD014894, 2011.

Ovadnevaite, J., Ceburnis, D., Martucci, G., Bialek, J., Monahan, C., Rinaldi, M., Facchini, M. C., Berresheim, H., Worsnop, D. R., and O'Dowd, C.: Primary marine organic aerosol: A dichotomy of low hygroscopicity and high CCN activity, Geophys. Res. Lett., 38, doi:10.1029/2011GL048869, 2011.

Piironen, P. and Eloranta, E.: Demonstration of a high-spectral-resolution lidar based on an iodine absorption filter, Opt. Lett., 19, 234–236, 1994.

Redemann, J., Vaughan, M. A., Zhang, Q., Shinozuka, Y., Russell, P. B., Livingston, J. M., Kacenelenbogen, M., and Remer, L. A.: The comparison of MODIS-Aqua (C5) and CALIOP (V2 & V3) aerosol optical depth, Atmos. Chem. Phys., 12, 3025–3043, doi:10.5194/acp-12-3025-2012, 2012.

Saxena, P., Hildemann, L. M., McMurry, P. H., and Seinfeld, J. H.: Organics alter hygroscopic behavior of atmospheric particles, J. Geophys. Res., 100, 18755–18770, doi:10.1029/95JD01835, 1995.

Sayer, A., Smirnov, A., Hsu, N., and Holben, B.: A pure marine aerosol model, for use in remote sensing applications, J. Geophys. Res., 117, doi:10.1029/2011JD016689, 2012.

Schuster, G. L., Vaughan, M., MacDonnell, D., Su, W., Winker, D., Dubovik, O., Lapyonok, T., and Trepte, C.: Comparison of CALIPSO aerosol optical depth retrievals to AERONET measurements, and a climatology for the lidar ratio of dust, Atmos. Chem. Phys., 12, 7431–7452, doi:10.5194/acp-12-7431-2012, 2012.

Shipley, S. T., Tracy, D., Eloranta, E. W., Trauger, J. T., Sroga, J., Roesler, F., and Weinman, J. A.: High spectral resolution lidar to measure optical scattering properties of atmospheric aerosols. 1: Theory and instrumentation, Appl. Opt., 22, 3716–3724, 1983.

Smirnov, A., Holben, B., Eck, T., Dubovik, O., and Slutsker, I.: Effect of wind speed on columnar aerosol optical properties at Midway Island, J. Geophys. Res., 108, 4802, doi:10.1029/2003JD003879, 2003.

Smirnov, A., Holben, B. N., Giles, D. M., Slutsker, I., O'Neill, N. T., Eck, T. F., Macke, A., Croot, P., Courcoux, Y., Sakerin, S. M., Smyth, T. J., Zielinski, T., Zibordi, G., Goes, J. I., Harvey, M. J., Quinn, P. K., Nelson, N. B., Radionov, V. F., Duarte, C. M., Losno, R., Sciare, J., Voss, K. J., Kinne, S., Nalli, N. R., Joseph, E., Krishna Moorthy, K., Covert, D. S., Gulev, S. K., Milinevsky, G., Larouche, P., Belanger, S., Horne, E., Chin, M., Remer, L. A., Kahn, R. A., Reid, J. S., Schulz, M., Heald, C. L., Zhang, J., Lapina, K., Kleidman, R. G., Griesfeller, J., Gaitley, B. J., Tan, Q., and Diehl, T. L.: Maritime aerosol network as a component of AERONET – first results and comparison with global aerosol models and satellite retrievals, Atmos. Meas. Tech., 4, 583–597, doi:10.5194/amt-4-583-2011, 2011.

Smirnov, A., Holben, B. N., Slutsker, I., Giles, D. M., McClain, C. R., Eck, T. F., Sakerin, S. M., Macke, A., Croot, P., Zibordi, G., Quinn P. K., Sciare, J., Kinne, S., Harvey, M., Smyth, T. J., Piketh S., Zielinski, T., Proshutinsky A., Goes, J. I., Nelson, N. B., Larouche, P., Radionov, V. F., Goloub, P., Krishna Moorthy, K., Matarrese, R., Robertson, E. J., and Jourdin, F.: Maritime Aerosol Network as a component of Aerosol Robotic Network, J. Geophys. Res., 114, D06204, doi:10.1029/2008JD011257, 2009.

Tesche, M., Ansmann, A., Müller, D., Althausen, D., Engelmann, R., Freudenthaler, V., and Groß, S.: Vertically resolved separation of dust and smoke over Cape Verde using multiwavelength Raman and polarization lidars during Saharan Mineral Dust Experiment 2008, J. Geophys. Res., 114, D13202, doi:10.1029/2009JD011862, 2009a.

Tesche, M., Ansmann, A., Müller, D., Althausen, D., Mattis, I., Heese, B., Freudenthaler, V., Wiegner, M., Esselborn, M., Pisani, G., and Knippertz, P.: Vertical profiling of Saharan dust with Raman lidars and airborne HSRL in southern Morocco during SAMUM, Tellus B, 61, 144–164, doi:10.1111/j.1600-0889.2008.00390.x, 2009b.

Vaughan, M. A., Young, S. A., Winker, D. M., Powell, K. A., Omar, A. H., Liu, Z., Hu, Y., and Hostetler, C. A.: Fully automated analysis of space-based lidar data: an overview of the CALIPSO retrieval algorithms and data products, Proc. SPIE, 5575, 16–30, doi:10.1117/12.572024, 2004.

Vaughan, M. A., Powell, K. A., Kuehn, R. E., Young, S. A., Winker, D. M., Hostetler, C. A., Hunt, W. H., Liu Z., McGill, M. J., and Getzewich, B. J.: Fully automated detection of cloud and aerosol layers in the CALIPSO lidar measurements, J. Atmos. Ocean Technol., 26, 2034–2050, doi:10.1175/2009JTECHA1228.1, 2009.

Wang, M. and Penner, J.: Aerosol indirect forcing in a global model with particle nucleation, Atmos. Chem. Phys., 9, 239–260, doi:10.5194/acp-9-239-2009, 2009.

Westervelt, D., Moore, R., Nenes, A., and Adams, P.: Effect of primary organic sea spray emissions on cloud condensation nuclei concentrations, Atmos. Chem. Phys., 12, 89–101, doi:10.5194/acp-12-89-2012, 2012.

Winker, D. M., Vaughan, M. A., Omar, A., Hu, Y., Powell, K. A., Liu, Z., Hunt, W. H., and Young, S. A.: Overview of the CALIPSO mission and CALIOP data processing algorithms, J. Atmos. Ocean. Technol., 26, 2310–2323, doi:10.1175/2009JTECHA1281.1, 2009.

Young, S. A., Cutten, D. R., Lynch, M. J., and Davies, J. E.: Lidar-derived variations in the backscatter-to-extinction ratio in southern hemisphere coastal maritime aerosols, Atmos. Environ., 27, 1541–1551, doi:10.1016/0960-1686(93)90154-Q, 1993.

Young, S. A. and Vaughan, M. A.: The retrieval of profiles of particulate extinction from cloud-aerosol lidar infrared pathfinder satellite observations (CALIPSO) data: algorithm description, J. Atmos. Oceanic Technol., 26, 1105–1119, doi:10.1175/2008JTECHA1221.1, 2009.